https://doi.org/10.5194/mr-2020-3
Preprint. Discussion started: 24 February 2020

Open Access MAGNETIC RESONANCE Discussions

Study of electron spectral diffusion process under DNP conditions by ELDOR spectroscopy focusing on the ^{14}N Solid Effect

Marie Ramirez Cohen, Akiva Feintuch, Daniella Goldfarb*, Shimon Vega*

[1]Department of Chemical Physics, Weizmann Institute of Science, Rehovot, Israel.

*Corresponding authors: Daniella Goldfarb (daniella.goldfarb@weizmann.ac.il), Shimon Vega (shimon.vega@weizmann.ac.il)

Abstract Electron spectral diffusion (eSD) plays an important role in solid state, static DNP with polarizers having in-homogeneously broadened EPR spectra, such as nitroxide radicals. It affects the electron spin polarization gradient within the EPR spectrum during microwave irradiation and thereby determines the effectiveness of the DNP process via the so called indirect cross effect (iCE) mechanism. The electron depolarization profile can be measured by Electron-Electron Double Resonance (ELDOR) experiments and a theoretical framework for deriving eSD parameters from ELDOR spectra and employing them to calculate DNP profiles has been developed. The inclusion of electron depolarization arising from the ^{14}N Solid Effect (SE) has not yet been taken into account in this theoretical framework and is the subject of the present work. The ^{14}N SE depolarization was studied using W-band ELDOR of a 0.5 mM TEMPOL solution, where eSD is negligible, taking into account the hyperfine interaction of both ^{14}N and ^{1}H nuclei, the long microwave irradiation applied under DNP conditions and electron and nuclear relaxation. The results of this analysis were then used in simulations of ELDOR spectra of 10 and 20 mM TEMPOL solutions, where eSD is significant using the eSD model and the SE contributions were added ad-hoc employing the ^{1}H and ^{14}N frequencies and their combinations, as found from the analysis of the 0.5 mM sample. This approach worked well for the 20 mM solution where a good fit for all ELDOR spectra recorded along the EPR spectrum was obtained and the inclusion of the ^{14}N SE mechanism improved the agreement with the experimental spectra. For the 10 mM solution, simulations of the ELDOR spectra recorded along the g_z position gave a lower quality fit than for spectra recorded in the center of the EPR spectrum, suggesting that the simple approach used to the SE of the ^{14}N contribution, when its contribution is high, is lacking as the anisotropy of its magnetic interactions has not been considered explicitly.

https://doi.org/10.5194/mr-2020-3
Preprint. Discussion started: 24 February 2020

Open Access MAGNETIC RESONANCE Discussions

1 Introduction

It has been recently recognized that electron spectral diffusion (eSD) plays a significant role in dynamic nuclear polarization (DNP) under static conditions(Hovav et al., 2015a; Leavesley et al., 2017) . It affects the electron spin polarization gradient within the EPR spectrum as a consequence of microwave irradiation and thereby determines the effectiveness of the DNP process via the so called indirect cross effect (iCE) mechanism(Hovav et al., 2015a). This is particularly relevant in the case of nitroxide radicals, the EPR spectra of which are in-homogeneously broadened in frozen solutions, at concentrations of 20-40 mM used in DNP applications. Hovav *et al* (Hovav et al., 2015b, 2015a), Siaw *et al*(Siaw et al., 2014) and Shimon *et al*(Shimon et al., 2012, 2014) observed that during constant microwave (MW) irradiation there exists an optimal radical concentration that leads to a maximum in the DNP enhancement. At this concentration the inter-electron spin dipolar interaction is sufficiently strong to generate a polarization gradient that favors an efficient iCE enhancement mechanism, while at higher concentrations the spectral diffusion saturates large parts of the EPR spectrum and spin temperature effects can be expected(Kundu et al., 2018a, 2018b). To monitor directly the electron depolarization during MW irradiation, Hovav *et al*(Hovav et al., 2015b) measured the ELDOR signals of frozen TEMPOL solutions under static DNP conditions, as a function of TEMPOL concentration, sample temperature and MW irradiation time. Furthermore, they developed a model (called the eSD model) that describes the depolarization process. This model is based on rate equations for the electron polarizations along the EPR spectrum, taking into account an exchange process between polarizations, in addition to the saturation effects of the MW irradiation and the spin-lattice relaxation. This eSD model introduces a fitting parameter Λ^{eSD} that defines the strength of the polarization exchange rate leading to the spectral diffusion within the EPR spectrum. Using this eSD model, experimental ELDOR spectra could be satisfactorily simulated and thus provide a feasible analytical description of the eSD process. Subsequently, it was demonstrated that once the polarization gradient within the EPR spectrum has been determined via the eSD model simulations, the lineshape of the associated DNP spectrum could be reproduced taking into account the polarization differences between all electron pairs satisfying the CE condition(Hovav et al., 2015a). This approach was also implemented by Leavesley *et al*, (Leavesley et al., 2017) when they explored the eSD process and its influence on the DNP efficiency

https://doi.org/10.5194/mr-2020-3
Preprint. Discussion started: 24 February 2020

Open Access MAGNETIC RESONANCE Discussions

at a magnetic field of 7T. They also considered the effects of variations in the radical concentration, temperature and MW power on the ^{1}H-DNP spectra. Furthermore, Kundu *et al.* used the eSD model to quantify the dependence of the electron polarization exchange parameter Λ^{eSD} on radical concentration and temperature[7].

To justify the rather phenomenological eSD model, Kundu *et al*(Kundu et al., 2018a, 2018b) performed quantum mechanical based calculations of the spin evolution and associated EPR spectra of the electron spins in dipolar coupled small spin systems under DNP conditions. In the case of weak dipolar coupling constants and adding cross relaxation(Hwang and Hill, 1967; Kessenikh et al., 1964) to the ELDOR calculations the results were similar to those obtained using the eSD model. In the case of strong dipolar couplings a Thermal Mixing mechanism in the rotating frame could provide the calculated EPR spectra under MW irradiation.(Abragam, 1961; de Boer, 1976; Borghini, 1968; Goldman, 1970; Provotorov, 1962; Wenckebach, 2016; Wollan, 1976) These studies also contributed to the validity of the iCE model in the weak and the strong coupling regime.

In addition to the CE mechanism, leading to the main nuclear signal enhancements at high radical concentrations, the Solid Effect (SE) process also influences these enhancements. This process contributes to the signal enhancements, but in addition causes some electron depolarization that in turn can influence the CE enhancement process(Hovav et al., 2015b; Leavesley et al., 2018). When nitroxide radicals are used as DNP polarizers, these SE depolarization effects arise from ^{1}H and ^{14}N nuclei hyperfine interactions(Kundu et al., 2018b; Leavesley et al., 2017). The SE induced polarization depletions are highly evident in ELDOR spectra at concentrations that are below the usual concentration used for DNP, but their influence is observed also at concentrations around 20 mM, which are relevant for DNP(Harris et al., 2011; Lilly Thankamony et al., 2017). As the ELDOR lineshapes are simulated for the determination of the Λ^{eSD} constants, the SE effects should be taken into account in the eSD model to ensure the extraction of their correct value. The purpose of this study is to account explicitly for the effects of the SE mechanism on ELDOR lineshapes for nitroxides and to explore its influence on the extraction of the Λ^{eSD} parameter at concentrations relevant for static DNP.

https://doi.org/10.5194/mr-2020-3
Preprint. Discussion started: 24 February 2020


Open Access MAGNETIC RESONANCE Discussions

We started this study by measuring ELDOR spectra of a 0.5 mM TEMPOL in DMSO frozen solution, in which the SE is the sole mechanism of depolarization, as the spectral diffusion mechanism is negligible. To analyze these ELDOR spectra we established a theoretical framework that accounts for all ^{14}N-SE and ^{1}H-SE depletions observed in these spectra. For this low concentration, the ELDOR spectrum is identical to the ELDOR detected NMR (EDNMR) spectrum of nitroxide, which has already been studied and simulated in the past(Cox et al., 2017; Florent et al., 2011; Kaminker et al., 2014; Nalepa et al., 2014, 2018). Yet, there is one major difference: Under EDNMR conditions, where resolution is of prime interest, the MW irradiation period is short, in the microsecond range, and therefore relaxation processes play a limited role during that irradiation. However, under DNP conditions the duration of the irradiation is in the range of milliseconds or longer and the electron and nuclear relaxation processes influence the magnitude of the depolarization. A second, more technical, difference is that in a full two dimensional (2D) EDNMR spectrum the EPR dimension is usually obtained by stepping the magnetic field(Kaminker et al., 2014; Ramirez Cohen et al., 2017), unless chirped pulses are being used(Wili and Jeschke, 2018), while 2D ELDOR maps in the context of DNP are obtained by stepping the frequency. Finally, so far contributions from different nuclei in the EDNMR spectra were taken into account by superimposing their individual spectra(Wang et al., 2018), ignoring the contributions of combination frequencies(Tan et al., 2019). Here we also account for ^{14}N-^{1}H combination lines in the ELDOR spectrum.

After analyzing the 0.5 mM spectrum, we proceeded to 10 and 20 mM TEMPOL solutions, where spectral diffusion becomes significant. We measured their ELDOR spectra and analyzed them employing the eSD model(Hovav et al., 2015b), taking into account the SE mechanism through an ad-hoc inclusion of the ^{14}N and ^{1}H frequencies.

2. Methods and Materials

2.1 Sample preparation

Samples of 2-3 µl in 0.6mm ID x 0.84 mm quartz tubes, with 0.5, 10 and 20 mM TEMPOL dissolved in a solution of DMSO/H_2O (1:1 v/v), were degassed by a *Freeze-Pump-Thaw* procedure and fast frozen with liquid Nitrogen. TEMPOL and DMSO were both purchased from Sigma Aldrich and used as is.

https://doi.org/10.5194/mr-2020-3
Preprint. Discussion started: 24 February 2020

Open Access MAGNETIC RESONANCE Discussions

2.2 Spectroscopic measurements

All measurements were carried out on our W-band (95 GHz, 3.4 T) homebuilt EPR spectrometer(Goldfarb et al., 2008; Mentink-Vigier et al., 2013) at 20 K.

Echo-detected EPR (ED-EPR) spectra were measured using the pulse sequence π/2-τ-π -τ-echo with τ=600 ns, while increasing the magnetic field stepwise from 3370 to 3395 mT, with a 2 ms repetition time. The pulse lengths were 100 ns for the π/2 pulse and 200 ns for the π pulse, optimized at the detection frequency (94.90 GHz).

Electron spin-lattice relaxation times T_{1e} were measured by saturation recovery experiments, using a long MW saturation pulse of 30 ms at different positions within the EPR spectrum and the echo was detected with low MW power as typical for DNP using two 300 ns pulses. The T_{1e} curves were analyzed using a superposition of two exponential functions with time constants t_1 and t_2, with the slow (and major) component assigned to T_{1e}.

ELDOR spectra were measured at different detection frequencies along the EPR line. The pulse sequence is shown in Figure 1. The spectrometer was set to low power as typical for DNP and therefore detection was performed by the sequence α-τ- α -τ-echo where α is a flip angle of less than π/2, While for EPR applications ELDOR is carried out at a fixed detection frequency and the magnetic field is varied to access different regions in the EPR spectrum, here we kept the field constant and varied the detection frequency to access the spectrum width as done for DNP applications. To carry out these ELDOR measurements, we increased the bandwidth of the cavity to accommodate the full spectrum of TEMPOL (approx. 500 MHz). The cavity resonance was tuned to 94.80 GHz. For the 0.5 mM sample ELDOR spectra (40 in total) were recorded as a function of the pump frequency, which was varied from 94.3 GHz to 95.3 GHz. To obtain two-dimensional ELDOR data the ELDOR spectrum was measured at

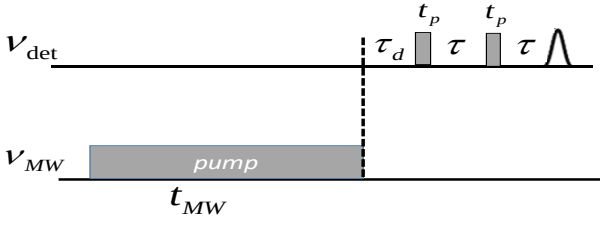

Figure 1. ELDOR pulse sequence, where ν_{det} is the detection frequency and ν_{MW} is the frequency of the pump pulse and t_{MW} is the duration of the pump pulse.

https://doi.org/10.5194/mr-2020-3
Preprint. Discussion started: 24 February 2020

Open Access MAGNETIC RESONANCE Discussions

different detection frequencies in intervals of 10 MHz from 94.55 GHz to 94.95 GHZ, which covers most of the EPR spectrum. The amplitude of the pump pulse, ν_1, was 0.5 MHz, as determined by a nutation experiment at 94.8 GHz, corresponding to an inversion pulse of 1µs. The experimental parameters for the ELDOR experiments are listed in **Table 1**.

Table 1. Parameters used in EDNMR experiment for 0.5, 10 and 20 mM radical concentration (see Fig. 1)

t_p	T	t_{MW}	Repetition time	τ_d
300 ns	600 ns	10 ms	20 ms	6 µs

3 Simulations

3.1 Low radical concentrations

The Hamiltonian and the allowed transition

In an effort to analyze the ELDOR spectra of the 0.5 nm TEMPOL solution we rely on quantum mechanical based calculations considering the spin evolution of a three-spin system consisting of an electron spin, S=1/2, coupled to a single ^{1}H nucleus and a single ^{14}N nucleus. Simulations of these ELDOR spectra were performed using a modified version of the computer code developed by Kaminker *et al*(Kaminker et al., 2014) for a two-spin system; one electron spin and one ^{14}N nucleus. The simulated ELDOR spectra comprise of EPR signals calculated at fixed detection frequency positions $\nu_{det} = \omega_{det} / 2\pi$ as a function of the of pump pulse frequency, $\nu_{MW} = \omega_{MW} / 2\pi$. During these calculations, we had to take into account the fact that the duration of the MW irradiation in DNP experiments t_{MW} is much longer than commonly used in EDNMR spectroscopy (ms vs µs range, respectively). For such long irradiation times the three-spin calculations cannot account for the experimental spectral observations, mainly due to the fact that the real spin system is more extended than only three spins because of the many coupled protons present in the sample. Accordingly, without extending the number of spins in our model we had to modify Kaminker's procedure to reproduce the experimental observations, as will be discussed here below.

The three-spin system is described by the following spin Hamiltonian in the MW rotating frame, assuming the high field approximation:

https://doi.org/10.5194/mr-2020-3
Preprint. Discussion started: 24 February 2020

Open Access MAGNETIC RESONANCE Discussions

$$\hat{H}_{\theta,\varphi} = \Delta\omega_e\hat{S}_z - \omega_N\hat{I}_{zN} - \omega_H\hat{I}_{zH} + A_{zz}^H\hat{S}_z\hat{I}_{zH} + A_{zz}^N\hat{S}_z\hat{I}_{zN} + (A_H^+\hat{I}_H^+ + A_H^-\hat{I}_H^-)\hat{S}_z + (A_N^+\hat{I}_N^+ + A_N^-\hat{I}_N^-)\hat{S}_z + \hat{I}_N\cdot\tilde{Q}\cdot\hat{I}_N \quad (1)$$

where

$$\Delta\omega_e\hat{S}_z = (\mu_B B_0 g_{eff}(\theta,\varphi) - \omega_{MW})\hat{S}_z \ . \quad (2)$$

In Eq. 1 we neglected the dipolar interaction between the nuclei. $\Delta\omega_e$ is the off-resonance electron frequency, B_0 is the strength of the external magnetic field, pointing along the z-axis of the laboratory frame, and $g_{eff}(\theta,\varphi)$ is the effective *g*-tensor parameter for a specific orientation of the magnetic field with respect to the principle axis system of the *g*-tensor, given by the polar angles θ and φ. The *g* tensor used for the calculation is *g* = [2.0065, 2.0037, 1.9997], obtained by simulating, using Easyspin(Stoll and Schweiger, 2006), the frequency domain EPR spectrum extracted from the echo intensity of the ELDOR spectra with the pump pulse set far outside the EPR spectrum (see Fig. S1 in ESI). The *g*-values obtained differ from those reported by Florent *et al*(Florent et al., 2011) (*g* = [2.00988, 2.00614, 2.00194]) and this seems to be due to a systematic error of 4 mT in the determination of the external magnetic field. The Larmor frequencies of ^{1}H and ^{14}N are $\omega_{\mathrm{H}} = 2\pi\nu_{\mathrm{H}}$ and $\omega_{\mathrm{N}} = 2\pi\nu_{\mathrm{N}}$, respectively. In the EPR high field approximation the terms that contribute to the hyperfine interaction are the secular and pseudo-secular terms with coefficients $(A_{zz}^{\mathrm{H}}, A_{\mathrm{H}}^{\pm})$ for ^{1}H and $(A_{zz}^{\mathrm{N}}, A_{\mathrm{N}}^{\pm})$ for ^{14}N, where $A_{\pm}^K = A_{zx}^K \pm iA_{zy}^K$, $K = \mathrm{H,N}$. In the case of ^{14}N the hyperfine tensor contains an isotropic contribution $a_{iso}^{\mathrm{N}} \neq 0$ in addition to the anisotropic tensor elements $[a_{ZZ}^K, a_{XX}^K, a_{YY}^K]$, where X, Y and Z are its principle axes. Assuming that the two anisotropic hyperfine interactions are of axial symmetry (i.e. $a_{XX}^K = a_{YY}^K = -1/2a_{ZZ}^K$) and that their major principal axes coincide with that of the *g*-tensor, the hyperfine coefficients of $\hat{H}_{\theta,\varphi}$ become $A_{zz}^K \equiv A_{zz}^K(\theta) = a_{iso}^K + \frac{1}{2}a_{ZZ}^K(3\cos^2\theta - 1)$ and $A_{\pm}^K \equiv A_{\pm}^K(\theta) = \frac{3}{2}a_{ZZ}^K\cos\theta\sin\theta$ (Schweiger and Jeschke, 2001). In the case of TEMPO, the isotropic ^{14}N contribution is $a_{iso}^{\mathrm{N}} = 44$ MHz and the anisotropic value is - $a_{ZZ}^{\mathrm{N}} = 55$ MHz. The ^{1}H hyperfine value was taken as is $a_{ZZ}^{\mathrm{H}} = 3$ MHz. Finally, the ^{14}N nuclear quadrupole interaction is also included in the spin Hamiltonian. Here we used the principal values of the quadrupole

https://doi.org/10.5194/mr-2020-3
Preprint. Discussion started: 24 February 2020

Open Access MAGNETIC RESONANCE Discussions

tensor obtained by Florent *et al*(Florent et al., 2011), $(Q_{XX}, Q_{YY}, Q_{ZZ}) = (0.48, 1.29, -1.77)$ MHz, and again assumed that its principal axes coincides with those of the *g*- tensor.

The MW irradiation Hamiltonian in the rotating frame is defined as

$$\hat{H}_{MW} = \omega_1 \hat{S}_x \ . \tag{3}$$

At the start of all our simulations, the Hamiltonian for each set of (θ,φ) angles is represented in matrix form, in the twelve product states of the basis sets in the laboratory frame $|\chi_e\rangle$, $|\chi_H\rangle$ with $\chi_{e,H} = \alpha, \beta$ and $|\chi_N\rangle$ with $\chi_N = +1, 0, -1$, and diagonalized according to

$$\hat{\Lambda}_{\theta,\varphi} = \hat{D}^{-1}_{\theta,\varphi} \hat{H}_{\theta,\varphi} \hat{D}_{\theta,\varphi} \quad . \tag{4}$$

$\hat{D}_{\theta,\varphi}$ is the diagonalization matrix and $\hat{\Lambda}_{\theta,\varphi}$ is the diagonal matrix consisting of the eigenvalues $E_i^{\theta,\varphi}$, in frequency units, corresponding to the 12 eigenstates $|\lambda_i^{\theta,\varphi}\rangle$ with $i = 1,,,12$. The EPR transition probabilities between levels $|\lambda_i^{\theta,\varphi}\rangle$ and $|\lambda_j^{\theta,\varphi}\rangle$ are :

$$P_{i,j}^{\theta,\varphi} = 2\left|\left\langle \lambda_i^{\theta,\varphi} \left| D^{-1}_{\theta,\varphi} \hat{S}_x D_{\theta,\varphi} \right| \lambda_j^{\theta,\varphi} \right\rangle\right|^2 . \tag{5}$$

When $|Q_{ZZ}| < \omega_N < \frac{1}{2} a_{ZZ}^N, a_{iso}$, the $\omega_n I_z^N$ term in all $H_{\theta,\varphi}$ Hamiltonians has little influence on the form of the eigenstates, which are products of the electron states $|\chi_e\rangle$ with the eigenvalues $m_e = \pm 1/2$, the hyperfine mixed proton states approximately equivalent to $|\chi_H\rangle$ with $m_H \approx \pm 1/2$ and the nitrogen states $|\chi_N\rangle$, mainly determined by the hyperfine interaction terms in $H_{\theta,\varphi}$ with $m_N \approx +1, 0, -1$. As a result we can easily recognize six "allowed" transition with frequencies $\nu_{(i,j)_a}(\theta,\varphi) = (E_i^{\theta,\varphi} - E_j^{\theta,\varphi})$ that correspond to EPR transitions $(i - j)_a$, with $\Delta m_e = \pm 1$, $\Delta m_H \approx 0$ and $\Delta m_N \approx 0$ and thus $P_{i,j}^{\theta,\varphi} \approx 1$. We note that for orientations along the X,Y axis, the ^{14}N hyperfine interaction is close to ω_N and therefore $P_{i,j}^{\theta,\varphi} < 1$. Figure 2 presents a schematic energy level diagram of the three-spin system for an arbitrary set of angles (θ,φ). The six allowed transitions are indicated by red arrows. For one of these transitions the corresponding homonuclear "single quantum"

https://doi.org/10.5194/mr-2020-3
Preprint. Discussion started: 24 February 2020

Open Access MAGNETIC RESONANCE Discussions

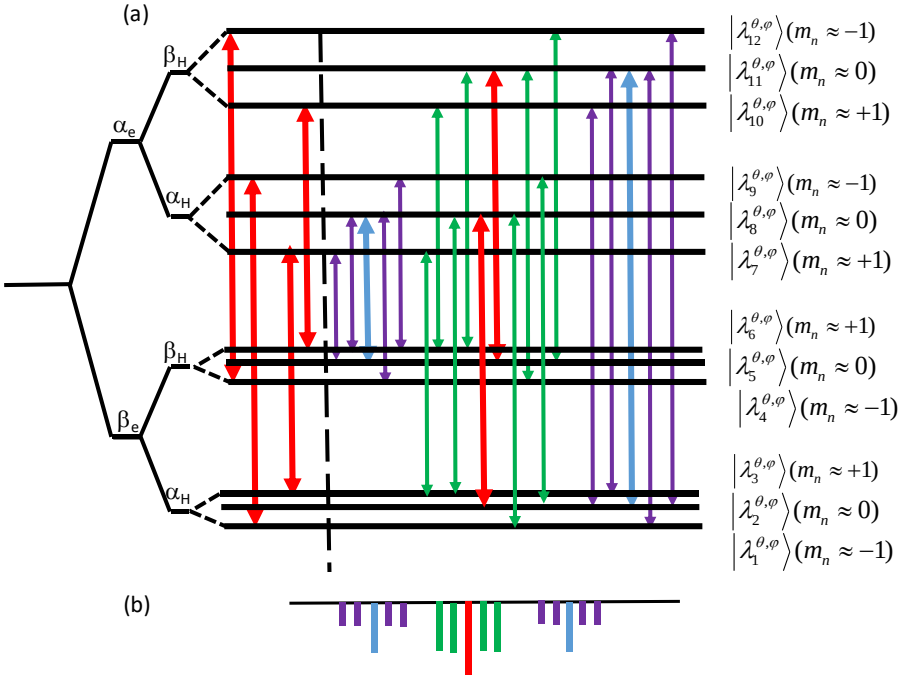

Figure 2. (a)A schematic energy level diagram of the three spin system with angles θ,φ , corresponding to an allowed transition. The eigenstates $|\lambda_i^{(\theta,\varphi)_{det}}\rangle$ are characterized by their m_N (** small n) values and product states of $|\chi_e\rangle$, $|\chi_H\rangle$ and $|\chi_N\rangle$. The energy level differences ν_e and $\nu_H \pm A_H$ are scaled arbitrarily. On the left of the energy level diagram the allowed transitions (3-7), (6-10) ,(1-9), (4-12) are indicated by the red arrows. On the right the red arrows correspond to the allowed transition between the states with sub-indexes (2-8) and (5-11). The nitrogen forbidden transitions (2-9), (2-7), (4-11) and (6-11) are assigned by the green arrow and the proton forbidden transitions (2-11) and (5-8) by the blue arrows. The purple arrows indicate the combined proton-nitrogen transitions. (b) A schematic presentation of the ELDOR spectrum of the allowed overlapping (2-8) and (5-11) transitions following the color coding of the arrows.

(SQ) forbidden transitions, with $\Delta m_H \approx \pm 1$ or $\Delta m_N \approx \pm 1$, are also indicated, in blue or green, respectively. The heteronuclear "double-" and "zero quantum" (DQ and ZQ) forbidden transitions, with $\Delta m_H \approx \pm 1$ and $\Delta m_N \approx \pm 1$, are shown in purple.

Using the Orisel function in Easyspin(Stoll and Schweiger, 2006), the values of $E_i^{\theta,\varphi}$ and $P_{i,j}^{\theta,\varphi}$ were calculated for a collection of 9609 sets of values of (θ,φ) and from them all transition frequencies $\nu_{i,j}(\theta,\varphi)$ were determined. To choose which orientations of the spin system contribute to the allowed EPR signal at a given ν_{det}, we search for those sets of angles (θ,φ) for which at least one allowed transition falls in the frequency

https://doi.org/10.5194/mr-2020-3
Preprint. Discussion started: 24 February 2020

Open Access MAGNETIC RESONANCE Discussions

range $\nu_{\rm det} - 3\text{MHz} \le \nu_{(i,j)_a}(\theta,\varphi) \le \nu_{\rm det} + 3\text{MHz}$. This frequency span provides a frequency bandwidth of 6 MHz for the detection pulse, estimated as the excitation bandwidth for a detection pulse of 300 ns length. In addition, it can account for some *g*- and hyperfine strain. This procedure generated a subset of selected $(\theta,\varphi)_{\rm det}$ pairs for each $\nu_{\rm det}$, the size of which depends on the position of $\nu_{\rm det}$ within the EPR spectrum. After choosing a value for $\nu_{\rm det}$ we simulated the ELDOR spectra of all crystal orientations of the subset $(\theta,\varphi)_{\rm det}$. The sum of these spectra are compared with the measured ELDOR spectrum at that frequency. To obtain the individual ELDOR spectra we calculated the EPR signal at $\nu_{\rm det}$ after a long MW pump pulse as a function of the frequency of this pulse, ν_{MW}.

The population rate equation

To follow the evolution of the spin system during the long MW irradiation period, prior to the EPR detection, it is sufficient to consider only the eigenstate populations $p_i^{\theta,\varphi}(t)$ of all $\left|\lambda_i^{\theta,\varphi}\right\rangle$, as described earlier (Hovav et al., 2010, 2015b). The rate equation during the MW irradiation for these populations can be presented as

$$\frac{d}{dt}p_i^{\theta,\varphi} = \sum_{j=1,12}\{-R_{ij}^{\theta,\varphi} + W_{ij}^{\theta,\varphi}\}p_j^{\theta,\varphi}, \qquad (6)$$

where $R_{ij}^{\theta,\varphi}$ are the elements of the 12x12 spin lattice relaxation matrix $\hat{R}_{\theta,\varphi}$ and $W_{ij}^{\theta,\varphi}$ are the elements of the 12x12 MW rate matrix $\hat{W}_{\theta,\varphi}$. The relaxation matrix $\hat{R}_{\theta,\varphi}$ is equal to the sum of the relaxation matrices $\hat{r}_{(ij)}^{\theta,\varphi}$ of all transitions $\{i-j\}$ with $E_j > E_i$. The non-zero matrix elements of $\hat{r}_{(ij)}^{\theta,\varphi}$ are derived, assuming a linear field fluctuation causing T_{1e}:

$$r_{(ij),ii}^{\theta,\varphi} = -\frac{1}{T_{1,ij}}\frac{1}{(1+\eta_{ij})} \quad ; \quad r_{(ij),ij}^{\theta,\varphi} = \frac{1}{T_{1,ij}}\frac{\eta_{ij}}{(1+\eta_{ij})}$$
$$r_{(ij),ji}^{\theta,\varphi} = \frac{1}{T_{1,ij}}\frac{1}{(1+\eta_{ij})}; \quad r_{(ij),jj}^{\theta,\varphi} = -\frac{1}{T_{1,ij}}\frac{\eta_{ij}}{(1+\eta_{ij})} \qquad (7a)$$

and

$$\frac{1}{T_{1,ij}} = \frac{\left|\left\langle\lambda_i^{\theta,\varphi}\left|\hat{S}_x\right|\lambda_j^{\theta,\varphi}\right\rangle\right|^2}{T_{1e}} \qquad (7b)$$

https://doi.org/10.5194/mr-2020-3
Preprint. Discussion started: 24 February 2020

Open Access MAGNETIC RESONANCE Discussions

with $\eta_{ij}^{\theta,\varphi} = p_i^{\theta,\varphi;eq} / p_j^{\theta,\varphi;eq}$ being the ratio between the thermal equilibrium populations and

$$\hat{R}_{\theta,\varphi} = \sum_{\{i-j\}} r_{(ij)}^{\theta,\varphi}. \tag{7c}$$

The elements of $\hat{W}_{\theta,\varphi}$ are equal to the sum of the $\hat{w}_{(ij)}^{\theta,\varphi}$ matrices with non-zero elements that express the effective irradiation strength on each transition $(i-j)$ (Hovav et al., 2010):

$$w_{(ij),ij}^{\theta,\varphi} = w_{(ij),ji}^{\theta,\varphi} = -w_{(ij),ii}^{\theta,\varphi} = -w_{(ij),jj}^{\theta,\varphi} = \frac{\omega_1^2 \left| \left\langle \lambda_i^{\theta,\varphi} \left| \hat{S}_x \right| \lambda_j^{\theta,\varphi} \right\rangle \right|^2 T_{2mw}}{1 + 4\pi^2 \left\{ \nu_{ij}^{\theta,\varphi} - \nu_{MW} \right\}^2 T_{2mw}^2} \tag{8a}$$

and

$$\hat{W}_{ij}^{\theta,\varphi} = \sum_{(i-j)} \hat{w}_{(ij)}^{\theta,\varphi}. \tag{8b}$$

Here ω_1 is the MW amplitude (see Eq. 3). A transverse relaxation time T_{2mw}, which determines the off-resonance efficiency of the irradiation, is introduced and for simplicity is assumed to be the same for all transitions. Note that T_{2mw} is not the measured phase memory time, T_M, which can serve as a lower limit for T_{2mw}. After choosing values for T_{1e}, ω_1 and an irradiation time, it is possible to solve Eq. 6 and to use the populations at the end of the irradiation to evaluate the EPR signals.

Setting the detection frequency at one of the allowed transition frequencies and irradiating with a pump frequency that matches one of its associated forbidden transitions (i.e, they share a common energy level) result in a depletion of the EPR signal. The calculations show that the depletion can be very significant for pump pulses on the order of tens of microseconds but disappears for irradiation periods of the order of tens of milliseconds. Thus using Eq. 6 works well for calculating EDNMR spectra for short pump pulses(Kaminker et al., 2014; Ramirez Cohen et al., 2017). However, for extended periods of MW irradiation, longer than T_{1e} as is applied in DNP, the simulated ELDOR signals reveal very weak signal at the forbidden transition frequencies. The reason for this is that for MW irradiations longer than T_{1e}, the SE spin evolution of an electron-nuclear spin pair brings the electronic polarization back to its equilibrium value. This is, however, in contrast to the experimental results where rather intense lines were observed even for long irradiation. The reason for this discrepancy

https://doi.org/10.5194/mr-2020-3
Preprint. Discussion started: 24 February 2020

Open Access MAGNETIC RESONANCE Discussions

is that in reality the electron spins are interacting with several equivalent coupled nuclei, which transfer their polarization to the bulk via nuclear spin diffusion. This is particularly true when many protons are present. Accordingly, to reproduce the experimental results, while still employing our simplified three-spin system model, requires modification of the simulation procedure as described next.

iii. Modification of the rate equation

In order to obtain from a three-spin calculations the observed EPR signal depletions even after long irradiation periods, we modified the form of the MW rate matrix. Realizing that an irradiation of one of the forbidden transitions, $(i-k)_f$ and $\underline{(k-j)_f}$, causes a depletion of the population difference of an allowed transition, $(i-j)_a$, we removed the four matrix elements of $\hat{w}^{\theta,\varphi}_{(ik)_f}$ and $\hat{w}^{\theta,\varphi}_{(kj)_f}$ from the $\hat{W}_{\theta,\varphi}$ matrix. This is equivalent to removing the irradiation on the forbidden transitions, which in turn cause the change in population difference of the allowed transition, $P^{\theta,\varphi}_{i,j}$. To re-introduce the effect of the forbidden transitions on $P^{\theta,\varphi}_{i,j}$ of the allowed transitions, we added reintroduced them as an artificial irradiation on the allowed one by adding them to the four non-zero matrix elements of $\hat{w}^{\theta,\varphi}_{(ij)_a}$: $\left\{\hat{w}^{\theta,\varphi}_{(ik)_f}+\hat{w}^{\theta,\varphi}_{(kj)_f}\right\}_{(ij)_a}$. In this way we ensure a depletion of the population difference of $(i-j)_a$, without the relaxation mechanism cancelling it. Realizing that the depletion during the simulations is now dependent on the value of $T_{i,ij}$, we introduce SE fitting parameters to adjust their values during irradiation: on for the different forbidden proton, a^{SE}_H, nitrogen, a^{SE}_N, combined proton-nitrogen, a^{SE}_{HN} and even double quantum (DQ) nitrogen, a^{SE}_{DQ-N} transitions. In this way an irradiation on $(i-k)_f$ reproduced the experimentally observed signal depletions, still taking into account the effective MW irradiation strengths, $\omega_1\times\left\langle\lambda^{\theta,\varphi}_i\middle|\hat{S}_x\middle|\lambda^{\theta,\varphi}_k\right\rangle$, and its original off resonance efficiency. Performing this procedure for all forbidden transitions, the modified $\hat{W}_{\theta,\varphi}$ matrix contains only elements corresponding to the allowed transitions $(i-j)_a$:

https://doi.org/10.5194/mr-2020-3
Preprint. Discussion started: 24 February 2020

Open Access MAGNETIC RESONANCE Discussions

$$\hat{W}_{\theta,\varphi} = \sum_{\substack{6\ allowed \\ (i-j)_a}} \hat{W}^{\theta,\varphi}_{(ij)_a} \quad ;$$

$$\hat{W}^{\theta,\varphi}_{(ij)_a} = \hat{w}^{\theta,\varphi}_{ij} + a^{SE}_{N} \sum_{(ik)_N;(kj)_N} \left\{ \hat{w}^{\theta,\varphi}_{(ik)_N} + \hat{w}^{\theta,\varphi}_{(kj)_N} \right\}_{(ij)_a} + a^{SE}_{DQ-N} \sum_{(ik)_{DQ-N};(kj)_{DQ-N}} \left\{ \hat{w}^{\theta,\varphi}_{(ik)_{DQ-N}} + \hat{w}^{\theta,\varphi}_{(kj)_{DQ-N}} \right\}_{(ij)_a}$$
$$+ a^{SE}_{H} \sum_{(ik)_H;(kj)_H} \left\{ \left\{ \hat{w}^{\theta,\varphi}_{(ik)_H} + \hat{w}^{\theta,\varphi}_{(kj)_H} \right\}_{(ij)_a} + a^{SE}_{HN} \sum_{(kl)_{HN};(lk)_{HN}} \left\{ \hat{w}^{\theta,\varphi}_{(kl)_{HN}} + \hat{w}^{\theta,\varphi}_{(lk)_{HN}} \right\}_{(ij)_a} \right\}$$

. (9)

Here the sums over k and l of $(ik)_K$, $(kj)_K$, $(kl)_{KK'}$, $(lk)_{KK'}$ are restricted to the homo-nuclear and hetero-nuclear forbidden transitions only. After this modification it becomes possible to write for each allowed transition $(i-j)_a$ a 2x2 rate equation for the populations $p^{\theta,\varphi}_i(i)$ and $p^{\theta,\varphi}_j(t)$ with a rate matrix $(-\hat{r}_{(ij)_a} + \hat{W}_{(ij)_a})$.

The actual relaxation pathways in the spin system is influenced by all the elements of $\hat{R}_{\theta,\varphi}$ and as a result, an irradiation on one allowed transition can have a small effect on the populations of another allowed transition.(Kaminker et al., 2014) Our modification caused this effect to vanish in the simulations. To reintroduce it in our simulations we added to each $\hat{W}^{\theta,\varphi}_{(ij)_a}$ the MW rate matrices of the other transitions $\hat{W}^{\theta,\varphi}_{(kl)_a}$, while introducing an additional small fitting parameter a_{a-a}:

$$\hat{W}^{\theta,\varphi}_{(ij)_a} = \hat{W}^{\theta,\varphi}_{(ij)_a} + a_{a-a} \sum_{\substack{(kl)_a \\ k,l \neq i,j}} \left\{ \hat{W}^{\theta,\varphi}_{(kl)_a} \right\}_{(ij)_a} \qquad (10)$$

Choosing values for all fitting parameters and inserting values for T_{1e} and T_{2mw}, the populations of the allowed transitions corresponding to $(\theta,\varphi)_{\text{det}}$ can now be obtained using Eq. 10 at the end of a MW pump period t_{MW} at frequency ν_{MW}. The EPR signal $\mathrm{E}_{\text{det}}(\nu_{\text{det}}, t_{MW})$ at ν_{det} can then be calculated by taking the Hamiltonian diagonalization into account and by solving Eq. 6 with the modified MW rate matrices for each set of angles (φ,θ). Adding all $(p^{\theta,\varphi}_{i_a} - p^{\theta,\varphi}_{j_a})(t_{MW})$ values belonging to $(\theta,\varphi)_{\text{det}}$ and normalizing their sum $S_{\text{det}}(\nu_{MW}, t_{MW})$ to the sum $S^{ref}_{\text{det}}(t_{MW})$ of all $(p^{\theta,\varphi}_{i_a} - p^{\theta,\varphi}_{j_a})(t_{MW})$ belonging to $(\theta,\varphi)_{\text{det}}$, obtained by again solving Eq. (10) but this time for a ν_{MW} value far removed from the frequency range of all allowed and forbidden transitions:

$$\mathrm{E}_{\text{det}}(\nu_{MW}, t_{MW}) = \mathrm{S}_{\text{det}}(\nu_{MW}, t_{MW}) / \mathrm{S}^{ref}_{\text{det}}(t_{MW}) \qquad (11).$$

https://doi.org/10.5194/mr-2020-3
Preprint. Discussion started: 24 February 2020

Open Access MAGNETIC RESONANCE Discussions

Plotting $E_{det}(\nu_{MW},t_{MW})$ as a function of ν_{MW}, and after line smoothing over 5 MHz, results in a ELDOR spectrum at ν_{det}. (see Fig. 2).

3.2 High radical concentrations

To simulate the ELDOR spectra of the 10 mM and 20 mM samples we used the eSD model (Hovav et al., 2015b). This computational model divides the EPR spectrum into frequency bins and calculates the electron polarizations $P_b(t_{MW})$ of each bin at frequency ν_b. It consists of a set of coupled rate equations for these polarizations with rate constants describing the effects of spin lattice relaxation, eSD polarization exchange and MW irradiation. To take the SE into account the MW rate constants of each $P_b(t_{MW})$, are extended by effective SE terms(Hovav et al., 2015b; Kundu et al., 2018b; Wang et al., 2018):

$$w_{MW}^{b}=\frac{\omega_1^2 T_{2mw}}{1+4\pi^2(\nu_b-\nu_{MW})^2T_{2mw}^2}+\sum_{K=H,N,H-N}\frac{(A_K^{SE}\omega_1)^2T_{2mw}}{1+4\pi^2(\nu_b\pm\nu_K-\nu_{MW})T_{2mw}^2}. \qquad (12)$$

Here ν_K are the ^{1}H and ^{14}N nuclear frequencies and A_H^{SE}, A_N^{SE} and A_{H-N}^{SE} are fitting parameters used to scale the MW power on the forbidden transition and just affect the SE peak intensities of the ELDOR peaks and not their positions. The eSD exchange rate constants between the polarizations in bin b and bin b' are defined by the exchange rate coefficients

$$r_{b,b'}^{eSD}=\frac{\Lambda^{eSD}}{4\pi^2(\nu_b-\nu_{b'})^2}, \qquad (13)$$

where the parameter Λ^{eSD} determines the time scale of the spectral diffusion process. After solving the polarization rate equations for an irradiation frequency ν_{MW} the polarization $P_{det}(\nu_{MW})$ at the detection frequency ν_{det} is obtained and divided by its Boltzman equilibrium value P_{det}^{eq} to obtain the ELDOR signal

$$E(\nu_{MW},\nu_{det},t_{MW})=\frac{P_{det}(\nu_{MW})}{P_{det}^{eq}} \qquad (14).$$

https://doi.org/10.5194/mr-2020-3
Preprint. Discussion started: 24 February 2020

Open Access MAGNETIC RESONANCE Discussions

4 Results and Discussion

4.1 ELDOR spectra of the 0.5 mM TEMPOL

Experimental ELDOR spectra of the 0.5 mM TEMPOL were obtained by recording EPR echo intensities as a function of ν_{MW} for fixed ν_{det} and t_{MW} values, using the experimental parameters summarized in the Experimental section. The results $\mathrm{E}(\nu_{MW};\nu_{\mathrm{det}},t_{MW})$ were analyzed using the procedure described in the Simulation section. From the many ELDOR spectra measured in this way, we show in Fig. 3 (black traces) only three, each one with a different detection frequency ν_{det} within the EPR spectrum. The dips in the ELDOR spectra, also referred to as EDNMR spectra, appear at the frequencies of the allowed and forbidden transitions, dictated by the ^{1}H and ^{14}N Larmor frequencies ν_H and ν_N and their hyperfine interactions $(A_{zz}^{H}, A_{H}^{\pm})$ for ^{1}H and $(A_{zz}^{N}, A_{N}^{\pm})$ for ^{14}N (Aliabadi et al., 2015; Cox et al., 2013, 2017; Kaminker et al., 2014; Nalepa et al., 2014; Ramirez Cohen et al., 2017; Rapatskiy et al., 2012). At W-band frequencies (~95 GHz) the ^{1}H frequencies are around 144 MHz and the ^{14}N frequencies are in the range $\approx 20-70\,\mathrm{MHz}$, as reported earlier in EDNMR experiments(Florent et al., 2011; Kaminker et al., 2014; Nalepa et al., 2014; Wili and Jeschke, 2018). Thus we expect in addition to the homo-nuclear forbidden transition signals additional signals around -144, 0 and +144 MHz each with a possible spread of -70 - +70 MHz, due to the hetero-nuclear forbidden transitions.

Fig. 3b shows the ELDOR spectrum for $\nu_{\mathrm{det}} = 94.55\,\mathrm{GHz}$. This frequency falls in the g_Z region of the EPR spectrum (Fig. 3a), which is characterized by its “single crystal like” features. As a result the ^{14}N signals are only slightly powder broadened and well resolved.(Florent et al., 2011; Kaminker et al., 2014) At this detection frequency the contributions to the echo signal originate only from the two low frequency allowed transitions (red in the $\Delta\nu_{\mathrm{det}} = -250$ MHz stick diagram), split by the ^{1}H hyperfine interaction, of the crystallites belonging to the “single crystal”. The MW excitation is not selective enough to resolve the protons splitting. In Table S1 in the supplementary the frequency assignments of the lines in the ELDOR spectra are correlated to the

https://doi.org/10.5194/mr-2020-3
Preprint. Discussion started: 24 February 2020

Open Access MAGNETIC RESONANCE Discussions

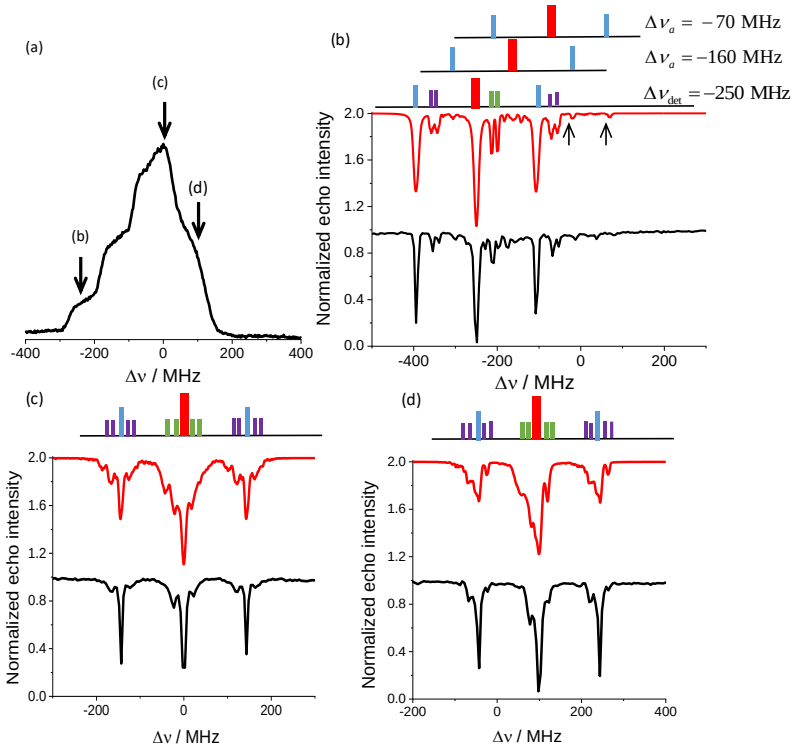

Fig. 3. (d) The EPR spectrum and the positions at which the ELDOR spectra shown in (b)-(d) were recorded. (d)-(d) Experimental (black) and simulated (red) ELDOR spectra along with the associated stick spectrum using the color codes shown in Fig. 2, with detection frequencies $\nu_{det} = 94.55, 94.8, 94.9$ GHz , for (b), (c), and (d) respectively. The frequency axis is plotted relative to the center of the EPR spectrum at 94.8GHz such that $\Delta\nu_{det} = -250$ MHz, 0MHz, 100MHz for (b), (c), and (d) respectively. The (b) spectrum is the most resolved , it shows the ^{14}N DQ transitions as well as peaks due to the other four allowed transitions and their associated ^{1}H forbidden transitions arising from off-resonance and relaxation effects..

$(i-j)_a$ and $(i-j)_f$ transitions in Fig. 2, together with the color coding in the stick spectrum shown in Fig. 3b. The assignments of the other four allowed transitions are also tabulated, together with their ^{1}H- and ^{14}N-homonuclear forbidden transitions and the ^{1}H-^{14}N-hetreonuclear forbidden transitions. In the ELDOR spectra the two ^{1}H-transitions (in blue) and the four ^{14}N-transitions (in green) are clearly present. The ^{1}H-^{14}N-transitions (in purple) are also detected. The additional spectral features must

https://doi.org/10.5194/mr-2020-3
Preprint. Discussion started: 24 February 2020

Open Access MAGNETIC RESONANCE Discussions

originate from the four non-directly detected allowed transitions with their forbidden transitions. Stick spectra of these allowed transitions and their ^{1}H-forbidden transitions are also added in Fig. 3a, and it is interesting to see that part of these lines in these spectra appear in the experimental ELDOR spectrum (marked by arrows in Fig. 3b). The appearance of signals corresponding to the no-directly excited allowed transition has been reported earlier(Kaminker et al., 2014) and was attributed to the combination of off-resonance and relaxation effects. In Fig. 3b the experimental ELDOR spectrum at $\nu_{\mathrm{det}} = 94.8\mathrm{GHz}$ (g_y) is plotted and a schematic stick spectrum is added on the top. All possible allowed transitions contribute to this spectrum and the spectral features are broadened and even hard to distinguish. The stick spectrum represents only one typical contribution to the observed powder spectrum. The same is true for the spectrum at $\nu_{\mathrm{det}} = 94.9\mathrm{GHz}$ (g_x).

To simulate the experimental ELDOR spectra we used the $T_{1\mathrm{e}}$ values, which were measured at several frequency positions within the EPR spectrum: 20.8ms at $\nu_{\mathrm{det}} = 94.6\mathrm{GHz}$, 13.8ms at $\nu_{\mathrm{det}} = 94.8\mathrm{GHz}$ and 15.8ms at $\nu_{\mathrm{det}} = 94.9\mathrm{GHz}$. Thus the $T_{1\mathrm{e}}$ values were found to vary with the position within the EPR spectrum, with the highest value obtained for the g_z region. In the simulations we used the average value of $T_{1e} = 16.7\mathrm{ms}$.

The best fit simulated spectra that resemble the three experimental ELDOR spectra in Fig. 3 are shown in red. To achieve these spectra we used the following parameters: $T_{2mw} = 100\ \mu\mathrm{s}$, $t_{MW} = 100\mathrm{ms}$ and the SE fitting parameters $a_H^{SE} = 10^3$, $a_N^{SE} = 0.5$, $a_{H-N}^{SE} = 10^3$ and $a_{a-a}^{SE} = 0.5\times10^{-3}$. These parameters were determined via manual fitting of the intensities of the different lines in the spectrum in Fig. 3b. The same parameters were used for the simulated spectra in Fig. 3c and 3d. The fact that the SE parameter of the ^{1}H-forbidden transitions is large, seems to be connected with the many protons involved in the SE process in the sample. In addition to the above mentioned forbidden transitions, we added also ^{14}N double quantum effect in the simulations by introducing a SE parameter of $a_{DQ}^{SE} = 5$. The resulting double quantum lines are shown in the simulated trace in Fig. 3a by small arrows. Comparing the simulated and experimental spectra we observe all expected forbidden transitions and some lines originating from the non-observed allowed transitions and their forbidden transitions. The double

https://doi.org/10.5194/mr-2020-3
Preprint. Discussion started: 24 February 2020

Open Access MAGNETIC RESONANCE Discussions

quantum lines expected around $\Delta\nu = 200$ MHz are not clearly resolved. The calculated spectra in Fig. 3c and 3d resemble the experimental spectra, although the relative intensities of the lines do not agree so well.

A contour plot of the experimental 2D-ELDOR spectrum of the 0.5 mM sample is shown in Fig. 4a. The positions of the lines corresponding to the allowed transitions appear at the intense central diagonal of the spectrum. The signals associated with the {e-^{14}N} forbidden transitions are close to the central diagonal and clearly reveal the anisotropic character of the hyperfine interaction. Namely, the strongest shifts of the line positions, with respect to the allowed line positions, are about 40 MHz in the g_z region of the EPR spectrum and they become around 20 MHz in the $g_{x,y}$ regime. The signals associated with the {e-^{1}H} forbidden transitions are the intense lines parallel to the diagonal, and are surrounded by the signals coming from the {e-^{1}H-^{14}N} forbidden transitions. Figure 4b shows the simulated 2D-ELDOR contour plot, which reproduces

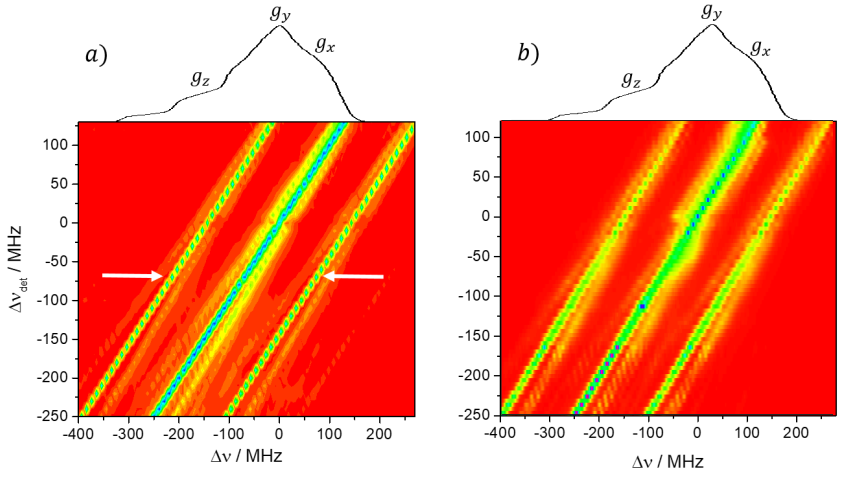

Figure 4. 2D contour ELDOR spectra of the 0.5mM sample (a) Experimental and (b) simulated spectra where the y-axis is the off-resonance detection frequency ($\Delta\nu_{det} = \nu_{det} - 94.8$ GHz) and the x-axis is the off-resonance pump frequency ($\Delta\nu_{mw}$). The central diagonal line corresponds to the allowed EPR transitions while the intense parallel lines on both its sides correspond to ^{1}H signals as indicated by white arrows in the experimental spectrum. The weaker lines around the center diagonal correspond to forbidden transitions involving ^{14}N and those about the outer ^{1}H lines are due to those involving both ^{1}H and ^{14}N

most of the features observed in the experimental contours. A notable discrepancy is

https://doi.org/10.5194/mr-2020-3
Preprint. Discussion started: 24 February 2020

Open Access MAGNETIC RESONANCE Discussions

the weaker ^{14}N signals on the negative side of the allowed transition, this is presumably a result of our choice of the co-alignment of the ^{1}H and ^{14}N hyperfine tensors.

4.2 ELDOR spectra of 10 mM and 20 TEMPOL

The 2D ELDOR spectrum for a 10 mM TEMPOL solution, presented in Fig. 5, displays the main features of the ^{1}H SE solid effect lines, which run parallel to the diagonal. ^{14}N and combination lines are detectable but they are not as nicely resolved as in the 0.5 mM sample. In addition, broad features that correspond to the depolarization of the electron spins owing to the eSD process are evident. To consider both SE and eSD effects we simulated the ELDOR spectra using the eSD model, including the influence of ^{14}N and ^{1}H SE by incorporating the SE features as described in the Simulation section Eq. 12. We also measured T_{1e} along the EPR spectrum and the results are given in Fig. 6. T_{1e} displays an anisotropic behavior, namely it depends on the position within the EPR spectrum with the largest variations observed in the g_z region (similar to our earlier observation for the 0.5 mM solution). Similar T_{1e} variations was also reported Weber *et al*(Weber et al., 2017).

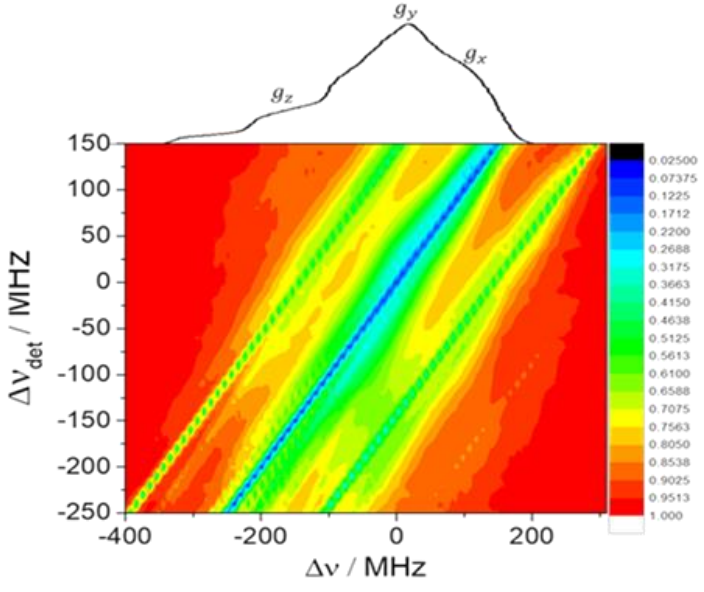

Figure 5: Experimental 2D ELDOR spectra of 10 mM TEMPOL solution

https://doi.org/10.5194/mr-2020-3
Preprint. Discussion started: 24 February 2020

Open Access MAGNETIC RESONANCE Discussions

To include the experimental T_{1e} values into the simulations, we assigned to each group of 5 consecutive bins, each one with a width of 2 MHz, the value of T_{1e} measured at the position in the EPR spectrum that correspond to those bins. Example of experimental and simulated ELDOR spectra for three positions of the detection frequency in the EPR spectrum are shown in Figure 7.

Initially the spectra were simulated using the eSD model considering only the ^{1}H SE effect (blue traces in Fig. 7), and the best fit gave an eSD parameter of $\Lambda^{eSD} = 60\ \mu s^{-3}$. A better fit was obtained when taking into account ^{14}N SE, including the ^{14}N-^{1}H combinations (green traces). This addition broadened the ELDOR lines resulting in a better match with the experimental result, with the same Λ^{eSD} value. Nevertheless, when ν_{det} reached the g_z region of the EPR spectrum (Fig. 7a, $\Delta\nu = -100$ MHz), the fit was not as good as in g_x and g_y. This implies that Λ^{eSD} might be anisotropic, which is unexpected. At this point we attribute this "apparent" anisotropy to the over simplified ad-hoc inclusion of the SE mechanism into the eSD model which does not fully account for the anisotropy of the ^{14}N hyperfine interaction. This is probably insufficient for reproducing the spectral features originating from the ^{14}N SE mechanism, which is highly anisotropic and has significant contributions at low concentrations, throughout the EPR spectrum.

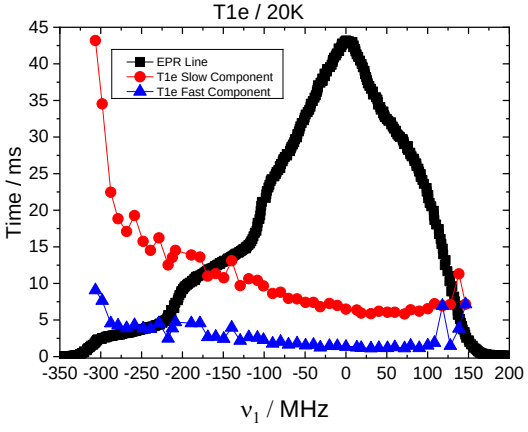

Figure 6. The frequency dependence of T_{1e} of 10 mM TEMPOL at 20K, measured every 10 MHz . Each point corresponds to a measurement fitted with a bi-exponential fit as noted on the figure.

https://doi.org/10.5194/mr-2020-3
Preprint. Discussion started: 24 February 2020

Open Access MAGNETIC RESONANCE Discussions

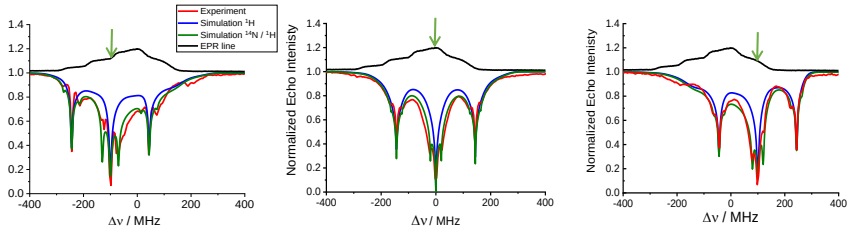

Figure 7. Experimental (red) and simulated (blue and green) ELDOR spectra of 10 mM TEMPOL at different positions along the EPR spectrum. All spectra were fitted with $\Lambda^{eSD} = 60\,\mu s^{-3}$, $T_{1e} = .7ms, T_2 = 100\mu s$. The blue spectra show the result of the simulation including only the ^{1}H SE while the green spectra include both ^{1}H and ^{14}N contributions. The detection frequency is marked with a green arrow at the top of each panel. The simulation was performed using 350 frequency bins with a 2 MHz width, spanning the whole EPR spectrum. The pump frequency spanned 1000 MHz with steps of 2 MHz, the forbidden transition fitting parameters were: $A_H^{SE} = 3\cdot10^{-3}, A_N^{SE} = 1.5\cdot10^{-3}, A_{HN}^{SE} = 0.4\cdot10^{-3}$. The NMR frequencies (corresponding the ν_K in Eq. 12) used in the simulation were $\omega_{H\_NMR} = \pm 144$ MHz, $\omega_{N\_NMR} = \pm 20$ MHz for ^{14}N, and $\omega_{HN\_NMR} = \omega_H \pm 20$ MHz for the ^{1}H and ^{14}N combinations.

To examine the degree of the influence of the ^{14}N SE on the electron depolarization at higher radical concentrations, where the ELDOR spectrum is shaped primarily by the eSD process, we tested also the 20 mM sample and used the eSD model to simulate the ELDOR lineshape recorded with ν_{det} set to the center of the EPR spectrum, as shown in Figure 8. Because of the high electron spin concentration, the eSD causes large depolarization of the EPR spectrum, which translates in extensive broadening of the ELDOR spectrum.

Figure 8 shows in red the experimental ELDOR spectrum, where although the lineshape of this spectrum is determined by the eSD process, we can still see small signals coming from the ^{14}N SE. Simulation including both the ^{1}H and ^{14}N SE with $\Lambda^{eSD} = 400\mu s^{-3}$ gave a good agreement with the experimental spectrum. In contrast, setting $\Lambda^{eSD} = 400\mu s^{-3}$ and taking into account only the contributions of the ^{1}H SE, did not result in a good fit. This shows that even at relative high radical concentrations, the effect of the

https://doi.org/10.5194/mr-2020-3
Preprint. Discussion started: 24 February 2020

Open Access MAGNETIC RESONANCE Discussions

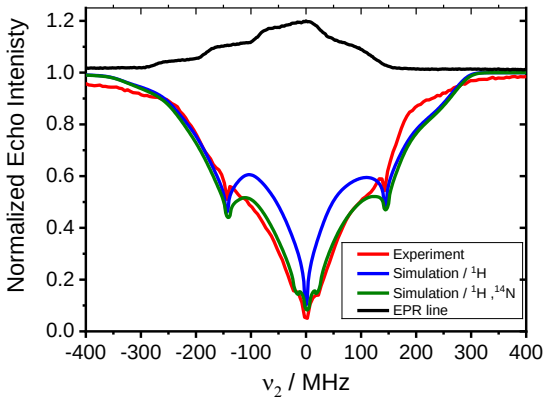

Figure 8. Experimental (red) and simulated (blue and green) ELDOR spectra of 20 mM TEMPOL recorded at the maximum of the EPR spectrum. The fit was achieved with $\Lambda^{eSD} = 400$ µs, $^{-3}$ $T_{1e} = 5.7ms, T_2 = 100\mu s$. The blue spectra show the result of the simulation including the only the ^{1}H SE while the green spectra include both ^{1}H and ^{14}N contributions. The forbidden transition fitting parameters were: $A_H^{SE} = 3\cdot10^{-3}, A_N^{SE} = 5\cdot10^{-3}, A_{HN}^{SE} = 0.4\cdot10^{-3}$ and the nuclear frequencies were the same as in Fig. 7.

depolarization due to the ^{14}N SE can still be significant and if not included can introduce inaccuracies in the eSD parameters and thus also in the DNP spectra, derived from the EPR lineshapes that are constructed using these parameters. Earlier measurements[7] showed that 20 mM TEMPOL concentration, ELDOR spectra measured at the g_y and g_z position gave the same quality fit with the same Λ^{eSD}, implying that at this concentration the relative contribution of the ^{14}N SE mechanism is small and can be accounted for by the simple model presented in this work.

5 Conclusions

In this work we focused on the contributions of the ^{14}N SE to the depolarization gradient within the EPR spectrum of TEMPOL, during long MW irradiation, as commonly used in DNP measurements, as determined by ELDOR measurements. For low concentration (0.5 mM) TEMPOL samples, where the SE dominates and eSD is negligible, we have successfully reproduced all the SE related depolarization signals, including those involving combinations of ^{1}H-^{14}N associated forbidden EPR transitions. Subsequently,

https://doi.org/10.5194/mr-2020-3
Preprint. Discussion started: 24 February 2020

Open Access MAGNETIC RESONANCE Discussions

we used the eSD model (Hovav et al., 2015c)(Hovav et al., 2015c)(Hovav et al., 2015c)(Hovav et al., 2015c) to simulate ELDOR spectra of 10 and 20 mM TEMPOL samples with ad-hoc addition of electron depolarization due to the ^{14}N SE based on the frequencies determined from the 0.5 mM sample. We observed that simulations including the ^{14}N SE improved the fit with experimental ELDOR spectra for the 10 mM sample. However we notice that at the g_z region of the EPR spectrum the fit is not as good indicating that the model is still not good enough to take into account the large ^{14}N SE contributions in this region. For the 20 mM concentration the effect is more drastic affecting significantly the best fitted value of Λ^{eSD} . We conclude that including ^{14}N SE in the eSD model is essential for obtaining reliable fitting at high radical concentrations.

Acknowledgments

This work is supported by a grant of the Binational Science Foundation (Grant #2014149) and was made possible in part by the historic generosity of the Harold Perlman Family (D. G.). D. G. holds the Erich Klieger Professorial Chair in Chemical Physics.

References

Abragam, A.: Principles of nuclear magnetism, Clarendon Press, Oxford, Oxford., 1961.

Aliabadi, A., Zaripov, R., Salikhov, K., Voronkova, V., Vavilova, E., Abdulmalic, M. A., Rüffer, T., Büchner, B. and Kataev, V.: Electron Spin Density on the N-Donor Atoms of Cu(II)-(Bis)oxamidato Complexes As Probed by a Pulse ELDOR Detected NMR, J. Phys. Chem. B, 119(43), 13762–13770, doi:10.1021/acs.jpcb.5b03987, 2015.

de Boer, W.: Dynamic orientation of nuclei at low temperatures, J. Low Temp. Phys., 22(1–2), 185–212, doi:10.1007/BF00655221, 1976.

Borghini, M.: Spin-Temperature Model of Nuclear Dynamic Polarization Using Free Radicals, Phys. Rev. Lett., 20(9), 419–421, doi:10.1103/PhysRevLett.20.419, 1968.

Cox, N., Lubitz, W. and Savitsky, A.: W band ELDOR detected NMR (EDNMR) spectroscopy as a versatile technique for the characterisation of transition metal ligand interactions, Mol. Phys., 111(18–19), 2788–2808, doi:10.1080/00268976.2013.830783, 2013.

Cox, N., Nalepa, A., Lubitz, W. and Savitsky, A.: ELDOR-detected NMR: A general and robust method for electron-nuclear hyperfine spectroscopy?, J. Magn. Reson., 280, 63–78, doi:10.1016/j.jmr.2017.04.006, 2017.

https://doi.org/10.5194/mr-2020-3
Preprint. Discussion started: 24 February 2020

Open Access MAGNETIC RESONANCE Discussions

1 Florent, M., Kaminker, I., Nagarajan, V. and Goldfarb, D.: Determination of the 14N
2 quadrupole coupling constant of nitroxide spin probes by W-band ELDOR-detected NMR, J.
3 Magn. Reson., 210(2), 192–199, doi:10.1016/j.jmr.2011.03.005, 2011.

4 Goldfarb, D., Lipkin, Y., Potapov, A., Gorodetsky, Y., Epel, B., Raitsimring, A. M., Radoul, M.
5 and Kaminker, I.: HYSCORE and DEER with an upgraded 95GHz pulse EPR spectrometer., J.
6 Magn. Reson., 194(1), 8–15, doi:10.1016/j.jmr.2008.05.019, 2008.

7 Goldman, M.: Spin temperature and magnetic resonance in solids, edited by (Oxford Univ.
8 Press, London., 1970.

9 Harris, T., Bretschneider, C. and Frydman, L.: Dissolution DNP NMR with solvent mixtures:
10 Substrate concentration and radical extraction, J. Magn. Reson., 211(1), 96–100,
11 doi:10.1016/j.jmr.2011.04.001, 2011.

12 Hovav, Y., Feintuch, A. and Vega, S.: Theoretical aspects of dynamic nuclear polarization in
13 the solid state - the solid effect., J. Magn. Reson., 207(2), 176–189,
14 doi:10.1016/j.jmr.2010.10.016, 2010.

15 Hovav, Y., Shimon, D., Kaminker, I., Feintuch, A., Goldfarb, D. and Vega, S.: Effects of the
16 electron polarization on dynamic nuclear polarization in solids, Phys. Chem. Chem. Phys.,
17 17(8), 6053–6065, doi:10.1039/C4CP05625F, 2015a.

18 Hovav, Y., Kaminker, I., Shimon, D., Feintuch, A., Goldfarb, D. and Vega, S.: The electron
19 depolarization during dynamic nuclear polarization: Measurements and simulations, Phys.
20 Chem. Chem. Phys., 17(1), 226–244, doi:10.1039/c4cp03825h, 2015b.

21 Hovav, Y., Kaminker, I., Shimon, D., Feintuch, A., Goldfarb, D. and Vega, S.: The electron
22 depolarization during dynamic nuclear polarization: Measurements and simulations, Phys.
23 Chem. Chem. Phys., 17(1), 226–244, doi:10.1039/c4cp03825h, 2015c.

24 Hwang, C. F. and Hill, D. A.: New effect in dynamic polarization, Phys. Rev. Lett., 18(4), 110–
25 112, doi:10.1103/PhysRevLett.18.110, 1967.

26 Kaminker, I., Wilson, T. D., Savelieff, M. G., Hovav, Y., Zimmermann, H., Lu, Y. and Goldfarb,
27 D.: Correlating nuclear frequencies by two-dimensional ELDOR-detected NMR spectroscopy.,
28 J. Magn. Reson., 240, 77–89, doi:10.1016/j.jmr.2013.12.016, 2014.

29 Kessenikh, A. V., Manenkov, A. A. and G.I., P.: On explanation of experimental data on
30 dynamic polarization of protons in irradiated polyethylenes, Sov. Physics-Solid State, 6(3),
31 641–643, 1964.

32 Kundu, K., Feintuch, A. and Vega, S.: Electron-Electron Cross-Relaxation and Spectral
33 Diffusion during Dynamic Nuclear Polarization Experiments on Solids, J. Phys. Chem. Lett.,
34 9(7), 1793–1802, doi:10.1021/acs.jpclett.8b00090, 2018a.

35 Kundu, K., Ramirez-Cohen, M., Feintuch, A., Goldfarb, D. and Vega, S.: Experimental
36 Quantification of Electron Spectral-Diffusion under static DNP conditions, Phys. Chem.
37 Chem. Phys., 478–489, doi:10.1039/C8CP05930F, 2018b.

38 Leavesley, A., Shimon, D., Siaw, T. A., Feintuch, A., Goldfarb, D., Vega, S., Kaminker, I. and
39 Han, S.: Effect of electron spectral diffusion on static dynamic nuclear polarization at 7 Tesla,
40 Phys. Chem. Chem. Phys., doi:10.1039/c6cp06893f, 2017.

41 Leavesley, A., Jain, S., Kamniker, I., Zhang, H., Rajca, S., Rajca, A. and Han, S.: Maximizing

https://doi.org/10.5194/mr-2020-3
Preprint. Discussion started: 24 February 2020

Open Access MAGNETIC RESONANCE Discussions

NMR signal per unit time by facilitating the e-e-n cross effect DNP rate, Phys. Chem. Chem. Phys., 20(43), 27646–27657, doi:10.1039/c8cp04909b, 2018.

Lilly Thankamony, A. S., Wittmann, J. J., Kaushik, M. and Corzilius, B.: Dynamic nuclear polarization for sensitivity enhancement in modern solid-state NMR, Prog. Nucl. Magn. Reson. Spectrosc., 102–103, 120–195, doi:10.1016/j.pnmrs.2017.06.002, 2017.

Mentink-Vigier, F., Collauto, A., Feintuch, A., Kaminker, I., Tarle, V. and Goldfarb, D.: Increasing sensitivity of pulse EPR experiments using echo train detection schemes, J. Magn. Reson., 236, 117–125, doi:10.1016/j.jmr.2013.08.012, 2013.

Nalepa, A., Möbius, K., Lubitz, W. and Savitsky, A.: High-field ELDOR-detected NMR study of a nitroxide radical in disordered solids:Towards characterization of heterogeneity of microenvironments in spin-labeled systems, Elsevier Inc., 2014.

Nalepa, A., Möbius, K., Plato, M., Lubitz, W. and Savitsky, A.: Nitroxide Spin Labels—Magnetic Parameters and Hydrogen-Bond Formation: A High-Field EPR and EDNMR Study, Appl. Magn. Reson., (0123456789), doi:10.1007/s00723-018-1073-3, 2018.

Provotorov, B. N.: Magnetic resonance saturation in crystals, Sov. Phys. JETP, 14(5), 1126–1131, 1962.

Ramirez Cohen, M., Mendelman, N., Radoul, M., Wilson, T. D., Savelieff, M. G., Zimmermann, H., Kaminker, I., Feintuch, A., Lu, Y. and Goldfarb, D.: Thiolate Spin Population of Type I Copper in Azurin Derived from 33 S Hyperfine Coupling, Inorg. Chem., 56(11), 6163–6174, doi:10.1021/acs.inorgchem.7b00167, 2017.

Rapatskiy, L., Cox, N., Savitsky, A., Ames, W. M., Sander, J., Nowaczyk, M. M., Rögner, M., Boussac, A., Neese, F., Messinger, J. and Lubitz, W.: Detection of the water-binding sites of the oxygen-evolving complex of photosystem II using W-band17O electron-electron double resonance-detected NMR spectroscopy, J. Am. Chem. Soc., 134(40), 16619–16634, doi:10.1021/ja3053267, 2012.

Schweiger, A. and Jeschke, G.: Principles of Pulse Electron Paramagnetic Resonance, Oxford University Press., 2001.

Shimon, D., Hovav, Y., Feintuch, A., Goldfarb, D. and Vega, S.: Dynamic Nuclear Polarization in the solid state: a transition between the cross effect and the solid effect., Phys. Chem. Chem. Phys., 14(16), 5729–43, doi:10.1039/c2cp23915a, 2012.

Shimon, D., Feintuch, A., Goldfarb, D. and Vega, S.: Static (1)H dynamic nuclear polarization with the biradical TOTAPOL: a transition between the solid effect and the cross effect., Phys. Chem. Chem. Phys., 16(14), 6687–6699, doi:10.1039/c3cp55504f, 2014.

Siaw, T. A., Fehr, M., Lund, A., Latimer, A., Walker, S. A., Edwards, D. T. and Han, S. I.: Effect of electron spin dynamics on solid-state dynamic nuclear polarization performance, Phys. Chem. Chem. Phys., 16(35), 18694–18706, doi:10.1039/c4cp02013h, 2014.

Stoll, S. and Schweiger, A.: EasySpin, a comprehensive software package for spectral simulation and analysis in EPR., J. Magn. Reson., 178(1), 42–55, doi:10.1016/j.jmr.2005.08.013, 2006.

Tan, K. O., Mardini, M., Yang, C., Ardenkjær-larsen, J. H. and Griffin, R. G.: Three-spin solid effect and the spin diffusion barrier in amorphous solids, Sci. Adv., (July), 1–8, 2019.

https://doi.org/10.5194/mr-2020-3
Preprint. Discussion started: 24 February 2020

Open Access MAGNETIC RESONANCE Discussions

1 Wang, X., McKay, J. E., Lama, B., Van Tol, J., Li, T., Kirkpatrick, K., Gan, Z., Hill, S., Long, J. R.
2 and Dorn, H. C.: Gadolinium based endohedral metallofullerene Gd2@C79N as a relaxation
3 boosting agent for dissolution DNP at high fields, Chem. Commun., 54(19), 2425–2428,
4 doi:10.1039/c7cc09765d, 2018.

5 Weber, E. M. M., Vezin, H., Kempf, J. G., Bodenhausen, G., Abergél, D. and Kurzbach, D.:
6 Anisotropic longitudinal electronic relaxation affects DNP at cryogenic temperatures, Phys.
7 Chem. Chem. Phys., 19(24), 16087–16094, doi:10.1039/c7cp03242k, 2017.

8 Wenckebach, T.: Essentials of Dynamic Nuclear Polarization, Spindrift Publications., 2016.

9 Wili, N. and Jeschke, G.: Chirp echo Fourier transform EPR-detected NMR, J. Magn. Reson.,
10 289, 26–34, doi:10.1016/j.jmr.2018.02.001, 2018.

11 Wollan, D. S.: Dynamic Nuclear Polarization with an inhomogeneously breoadened ESR line.
12 I. Theory, Phys. Rev. B, 13(9), 1976.

13

14

15

16